Phase sensitive amplification based on quadratic cascading in a periodically poled lithium niobate waveguide

Kwang Jo Lee,[1,*] Francesca Parmigiani,[1] Sheng Liu,[1] Joseph Kakande,[1] Periklis Petropoulos,[1] Katia Gallo,[2] and David Richardson[1]

[1]*Optoelectronics Research Centre, University of Southampton, Southampton, SO17 1BJ, United Kingdom*
[2]*Department of Applied Physics, Royal Institute of Technology (KTH), 10691 Stockholm, Sweden*
[*] *kjl@orc.soton.ac.uk*

Abstract: We propose and demonstrate phase-sensitive amplification based on cascaded second harmonic generation and difference frequency generation within a periodically poled lithium niobate waveguide. Excellent agreement between our numerical simulations and proof-of-principle experiments using a 3-cm waveguide device operating at wavelengths around 1550 nm is obtained. Our experiments confirm the validity and practicality of the approach and illustrate the broad gain bandwidths achievable. Additional simulation results show that the maximum gain/attenuation factor increases quadratically with input pump power, reaching a value of ±19.0dB at input pump powers of 33 dBm for a 3 cm-long waveguide. Increased gains/reduced powers for a fixed gain could be achieved using longer crystals.

OCIS codes: (130.3730) Lithium niobate; (190.4410) Nonlinear optics, parametric processes; (190.4970) Parametric oscillators and amplifiers; (230.2285) Fiber devices and optical amplifiers; (230.4320) Nonlinear optical devices; (230.4480) Optical amplifiers.

References and links

1. C. M. Caves, "Quantum limits on noise in linear amplifiers," Phys. Rev. D **26**, 1817-1839 (1982).
2. J. A. Levenson, I. Abram, T. Rivera, and P. Grainger, "Reduction of quantum-noise in optical parametric amplification," J. Opt. Soc. Am. B **10**, 2233-2238 (1993).
3. Z. Y. Ou, S. F. Pereira, and H. J. Kimble, "Quantum noise reduction in optical amplification," Phys. Rev. Lett. **70**, 3239-3242 (1993).
4. K. Croussore, I. Kim, Y. Han, C. Kim, G. Li, and S. Radic, "Demonstration of phase-regeneration of DPSK signals based on phase-sensitive amplification," Opt. Express **13**, 3945-3950 (2005).
5. K. Croussore and G. Li, "Phase and amplitude regeneration of differential phase-shift keyed signals using phase-sensitive amplification," IEEE J. Sel. Topics Quantum Electron. **14**, 648-658 (2008).
6. R. -D. Li, P. Kumar, and W. L. Kath "Dispersion compensation with phase-sensitive optical amplifiers," J. Lightwave Technol. **12**, 541-549 (1994).
7. W. Imajuku and A. Takada, "Reduction of fiber-nonlinearity-enhanced amplifier noise by means of phase-sensitive amplifiers," Opt. Lett. **22**, 31-33 (1997).
8. D. J. Lovering, J. A. Levenson, P. Vidakovic, J. Webjörn, and P. St. J. Russell, "Noiseless optical amplification in quasi-phase-matched bulk lithium niobate," Opt. Lett. **21**, 1439-1441 (1996).
9. T. Tajima, Y. Etou, T. Hirano, "Parametric amplification in a periodically poled lithium niobate waveguide at telecommunication wavelength," in Proceedings of International Quantum Electronics Conference (Toshi Center Hotel Tokyo, 2005), pp. 1131-1132.
10. Y. Eto, T. Tajima, Y. Zhang, and T. Hirano, "Observation of squeezed light at 1.535 μm using a pulsed homodyne detector," Opt. Lett. **32**, 1698-1700 (2007).
11. Y. Eto, T. Tajima, Y. Zhang, and T. Hirano, "Observation of quadrature squeezing in a $\chi^{(2)}$ nonlinear waveguide using a temporally shaped local oscillator pulse," Opt. Express **16**, 10650-16657 (2008).
12. H. P. Yuen and J. H. Shapiro, "Generation and detection of two-photon coherent states in degenerate four-wave mixing," Opt. Lett. **4**, 334-336 (1979).
13. P. Kumar and J. H. Shapiro, "Squeezed-state generation via forward degenerate four-wave mixing," Phys. Rev. A **30**, 1568-1571 (1984).

14. C. J. McKinstrie and S. Radic, "Phase-sensitive amplification in a fiber," Opt. Express **12**, 4973-4979 (2004).
15. R. Tang, J. Lasri, P. S. Devgan, V. Grigoryan, P. Kumar, and M. Vasilyev, "Gain characteristics of a frequency nondegenerate phase-sensitive fiber-optic parametric amplifier with phase self-stabilized input," Opt. Express **13**, 10483-10493 (2005).
16. R. Tang, P. S. Devgan, V. S. Grigoryan, P. Kumar, and M. Vasilyev, "In-line phase-sensitive amplification of multi-channel CW signals based on frequency nondegenerate four-wave-mixing in fiber," Opt. Express **16**, 9046-9053 (2008).
17. C. Lundström, J. Kakande, P. A. Andrekson, P. Petropoulos, F. Parmigiani, and D. J. Richardson, "Experimental comparison of gain and saturation characteristics of a parametric amplifier in phase-sensitive and phase-insensitive mode," presented at the European Conference on Optical Communication, Austria Center Vienna, Vienna, 20-24 Sept. 2009.
18. C. Langrock, S. Kumar, J. E. McGeehan, A. E. Willner, and M. M. Fejer, "All-optical signal processing using $\chi^{(2)}$ nonlinearities in guided-wave devices," J. Lightwave Technol. **24**, 2579-2592 (2006).
19. K. Gallo, G. Assanto, and G. I. Stegeman, "Efficient wavelength shifting over the erbium amplifier bandwidth via cascaded second order processes in lithium niobate waveguides," Appl. Phys. Lett. **71**, 1020-1022 (1997).
20. M. H. Chou, I. Brener, M. M. Fejer, E. E. Chaban, and S. B. Christman, "1.5-μm-band wavelength conversion based on cascaded second-order nonlinearity in $LiNbO_3$ waveguides," IEEE Photon. Technol. Lett. **11**, 653-655 (1999).
21. J. Wang, J. Sun, X. Zhang, and D. Huang, "All-optical tunable wavelength conversion with extinction ratio enhancement using periodically poled lithium niobate waveguides," J. Lightwave Technol. **26**, 3137-3148 (2008).
22. J. Wang, J. Sun, X. Zhang, D. Huang, and M. M. Fejer, "All-optical format conversions using periodically poled lithium niobate waveguides," IEEE J. Quantum Electron. **45**, 195-205 (2009).
23. J. E. McGeehan, M. Giltrelli, and A. E. Willner, "All-optical digital 3-input AND gate using sum- and difference-frequency generation in a PPLN waveguide," Electron. Lett. **43**, 409-410 (2007).
24. H. Ishizuki, T. Suhara, M. Fujimura, and H. Nishihara, "Wavelength conversion type picosecond optical switching using a waveguide QPM-SHG/DFG device," Opt. Quantum Electron. **33**, 953-961 (2001).
25. Y. Wang, C. Yu, L. Yan, A. E. Willner, R. Roussev, C. Langrock, M. M. Fejer, J. E. Sharping, and A. L. Gaeta, "44-ns continuously tunable dispersionless optical delay element using a PPLN waveguide with two-pump configuration, DCF, and a dispersion compensator," IEEE Photon. Technol. Lett. **19**, 861-863 (2007).
26. K. Gallo and G. Assanto, "Analysis of lithium niobate all-optical wavelength shifters for the third spectral window," J. Opt. Soc. Am. B **16**, 741-53 (1999).
27. C. Liberale, I. Cristiani, L. Razzari, and V. Degiorgio, "Numerical study of cascaded wavelength conversion in quadratic media," J. Opt. A **4**, 457-462 (2002).
28. Ichiro Shoji, Takashi Kondo, Ayako Kitamoto, Masayuki Shirane, and Ryoichi Ito, "Absolute scale of second-order nonlinear-optical coefficients," J. Opt. Soc. Am. B **14**, 2268-2294 (1997).
29. J. A. Armstrong, N. Bloembergen, J. Ducuing, and P. S. Pershan, "Interactions between light waves in a nonlinear dielectric," Phys. Rev. **127**, 1918-1939 (1962).
30. S. -K. Choi, M. Vasilyev, and P. Kumar, "Noiseless optical amplification of images," Phys. Rev. Lett. **83**, 1938-1941 (1999).

1. Introduction

Optical amplifiers such as erbium-doped-fibre amplifiers (EDFAs), semiconductor optical amplifiers (SOAs), and Raman amplifiers are in common use in optical communication and sensor systems. These amplifiers are examples of phase-insensitive amplifiers (PIAs), since their gain does not depend on the optical phase of the input signals [1]. In theory one could also use phase-sensitive amplifiers (PSAs), which are capable of amplifying or deamplifying input signals according to the phase of the optical signal [2, 3]. One of the most intriguing advantages of PSAs is that the noise figure can potentially be reduced below the 3dB quantum limit of PIAs. Other advantages are the potential for optical phase and amplitude regeneration [4, 5], dispersion compensation [6], and the suppression of modulational instability [7]. Various schemes to achieve PSA have been reported previously, including degenerate parametric amplification (PA) (or squeezed-state generation) in a $\chi^{(2)}$ medium [8-11] and degenerate four-wave mixing (FWM) in a $\chi^{(3)}$ medium [12-14]. In Ref. [8], direct optical parametric amplification in a bulk PPLN sample was used to realize frequency degenerate PSA, however this approach requires a pump laser operating in the wavelength range 750-800 nm in order to be applied to signals in the telecommunication band. This particular approach

is problematic not only because it needs a pump laser outside of the communication bands but also because telecom waveguides are typically multimode for inputs in the very near infrared, which implies significant insertion losses for a direct DFG $\chi^{(2)}$ waveguide-based PSA. Alternative $\chi^{(3)}$ PSA schemes based on nonlinear fibre optic PAs have been more widely investigated, with recent demonstration of frequency non-degenerate schemes offering potential important advantages relative to their frequency degenerate counterparts [15-17]. In particular, frequency non-degenerate PSAs can be operated as multi-channel devices, which are compatible with wavelength-division multiplexing (WDM) system.

In recent years, the use of cascaded second-order nonlinearities in periodically poled lithium niobate (PPLN) waveguides has attracted considerable interest as another promising route to realise all-optical signal processing. Their advantages include amongst others a high nonlinear coefficient, ultra-fast optical response, transparency to bit rate and modulation format, low spontaneous emission noise, low cross talk, and no intrinsic frequency chirp [18]. Two kinds of cascaded second-order nonlinear interactions: cascaded second-harmonic and difference-frequency generation (cSHG/DFG), and cascaded sum- and difference-frequency generation (cSFG/DFG), have been exploited in various applications in all-optical signal processing including all-optical wavelength conversion [19-21], format conversion [22], logic gates [23], switching [24], and tunable optical delay lines [25].

In this paper, we report a new scheme for frequency non-degenerate PSA based on the cSHG/DFG process in a PPLN waveguide. We will describe in detail the theoretical model developed for the quadratic cascading interaction, and then experimentally validate our model. PPLN-based PSA offers a number of attractive features relative to fibre-based PSA implementations including the prospect of compact devices, low-latency, large operational bandwidths, and importantly a far greater immunity to the effects of Stimulated Brillouin Scattering (SBS) of the pump beams which imposes performance limitations and adds complexity to silica fibre-based PSA devices.

2. Theoretical model

Figure 1 shows the schematic diagram of the cSHG/DFG interaction in a single PPLN waveguide for frequency non-degenerate PSA. Three waves: a pump, a signal, and an idler, with frequencies of ω_p, ω_s, and ω_i are injected with a fixed phase relation into the waveguide [15-17]. The pump generates a wave at the second harmonic frequency ($2\omega_p$), which interacts with the other input waves via the DFG process ($\omega_i = 2\omega_p - \omega_s$).

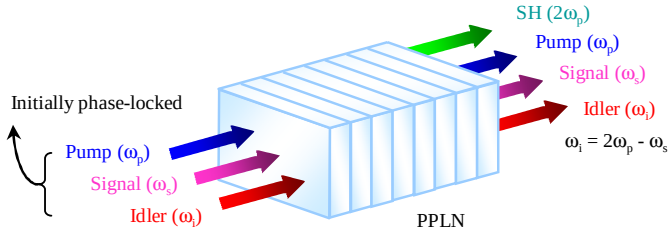

Fig. 1. Schematic diagram of the cSHG/DFG process in a PPLN waveguide. The relative phases among the input waves need to be initially locked.

Under the slowly varying envelope approximation, the coupled-mode equations describing the cSFG/DFG process can be derived as follows [26, 27]:

$$\frac{dE_p(z)}{dz} = -\frac{\alpha_p}{2}E_p(z) + i\kappa_{pp}\omega_p E_{SH}(z)E_p^*(z)e^{i\Delta k_{pp}z}, \tag{1}$$

$$\frac{dE_{SH}(z)}{dz} = -\frac{\alpha_{SH}}{2}E_{SH}(z) + i\kappa_{pp}\omega_p E_p^2(z)e^{-i\Delta k_{pp}z} + 2i\kappa_{si}\omega_p E_s(z)E_i(z)e^{i\Delta k_{si}z}, \tag{2}$$

$$\frac{dE_s(z)}{dz} = -\frac{\alpha_s}{2}E_s(z) + i\kappa_{si}\omega_s E_{SH}(z)E_i^*(z)e^{-i\Delta k_{si}z}, \tag{3}$$

$$\frac{dE_i(z)}{dz} = -\frac{\alpha_i}{2}E_i(z) + i\kappa_{si}\omega_i E_{SH}(z)E_s^*(z)e^{-i\Delta k_{si}z}, \tag{4}$$

where E_p, E_{SH}, E_s, and E_i denote the normalized complex electric fields of the pump, SH, signal, and idler waves propagating along the axis (z) of the waveguide, respectively. Each α represents the linear propagation loss coefficients for the corresponding wave. The coupling coefficients for the SHG (κ_{pp}) and the DFG process (κ_{si}) are expressed as,

$$\kappa_{pp} = d_{eff}\sqrt{\frac{2\mu_0}{cn_p^2 n_{SH}A_{eff}}}, \tag{5}$$

$$\kappa_{si} = d_{eff}\sqrt{\frac{2\mu_0}{cn_s n_i n_{SH}A_{eff}}}, \tag{6}$$

where, d_{eff}, μ_0, c, A_{eff}, and n_j represent the effective nonlinear coefficient, the permeability of free space, the speed of light, the effective mode area in the PPLN waveguide (assumed to be the same for the SHG and DFG cases), and the refractive indices of each wave, respectively. For a type-0 QPM geometry, which is the one we considered, d_{eff} is given by $(2/\pi)d_{33}$ (d_{33} = 25 pm/V for the SHG at 1064 nm) [28]. The phase mismatches for the SHG (Δk_{pp}) and the DFG processes (Δk_{si}) are expressed as,

$$\Delta k_{pp} = k_{SH} - 2k_p - \frac{2\pi}{\Lambda}, \tag{7}$$

$$\Delta k_{si} = k_s + k_i - k_{SH} + \frac{2\pi}{\Lambda}, \tag{8}$$

where, Λ is the period of QPM grating and each k is the wave vector at the corresponding frequency. The coupled wave equations [Eqs. (1) - (4)] can be conveniently rewritten in terms of amplitudes and phases of the waves by introducing the following complex notation as in [29],

$$E_j(z) \equiv A_j(z)e^{i\phi_j(z)}, \tag{9}$$

where, A_j and ϕ_j denote the modulus and phase of the complex field amplitude for a generic interacting wave j, respectively. If we substitute Eq. (9) into Eqs. (1) - (4), the coupled wave equations can be expressed as the following set of six equations:

$$\frac{dA_p(z)}{dz} = -\frac{\alpha_p}{2}A_p(z) - \kappa_{pp}\omega_p A_{SH}(z)A_p(z)\sin\theta(z), \tag{10}$$

$$\frac{dA_{SH}(z)}{dz} = -\frac{\alpha_{SH}}{2}A_{SH}(z) + \kappa_{pp}\omega_p A_p^2(z)\sin\theta(z) - 2\kappa_{si}\omega_p A_s(z)A_i(z)\sin\psi(z), \tag{11}$$

$$\frac{dA_s(z)}{dz} = -\frac{\alpha_s}{2}A_s(z) + \kappa_{si}\omega_s A_{SH}(z)A_i(z)\sin\psi(z), \tag{12}$$

$$\frac{dA_i(z)}{dz} = -\frac{\alpha_i}{2} A_i(z) + \kappa_{si}\omega_i A_{SH}(z) A_s(z) \sin\psi(z), \tag{13}$$

$$\begin{aligned}\frac{d\theta(z)}{dz} = &\left(\kappa_{pp}\omega_p \frac{A_p^2(z)}{A_{SH}(z)} - 2\kappa_{pp}\omega_p A_{SH}(z) \right) \cos\theta(z) \\ &+ 2\kappa_{si}\omega_p \frac{A_s(z)A_i(z)}{A_{SH}(z)} \cos\psi(z) + \Delta k_{pp},\end{aligned} \tag{14}$$

$$\begin{aligned}\frac{d\psi(z)}{dz} = &\left(\kappa_{si}\omega_s \frac{A_{SH}(z)A_i(z)}{A_s(z)} + \kappa_{si}\omega_i \frac{A_{SH}(z)A_s(z)}{A_i(z)} - 2\kappa_{si}\omega_p \frac{A_s(z)A_i(z)}{A_{SH}(z)} \right) \cos\psi(z) \\ &- \kappa_{pp}\omega_p \frac{A_p^2(z)}{A_{SH}(z)} \cos\theta(z) + \Delta k_{si},\end{aligned} \tag{15}$$

where, two kinds of relative phase relationship between the interacting waves can also be defined as follows:

$$\theta(z) \equiv \phi_{SH}(z) - 2\phi_p(z) + \Delta k_{pp} z, \tag{16}$$

$$\psi(z) \equiv \phi_s(z) + \phi_i(z) - \phi_{SH}(z) + \Delta k_{si} z. \tag{17}$$

Here, θ and ψ denote the relative phase variation between the interacting waves in the beam propagation direction (z) for the SHG and DFG processes, respectively.

The coupled-mode equations [Eqs. (10) - (15)] were numerically solved by considering the same parameters for the PPLN waveguide (HC Photonics Corp.) that we use in the experiments described in the following section. The PPLN waveguide was designed for SHG at the pump wavelength (λ_p) of 1546.0 nm, while the signal (λ_s) and idler (λ_i) wavelengths are set at 1541.4 nm and 1550.6 nm, respectively. The effective mode area and the linear loss coefficients for the PPLN waveguide are A_{eff} = 52 μm^2, $\alpha_p = \alpha_s = \alpha_i$ = 0.35 dB/cm, and α_{SH} = 0.7 dB/cm, respectively. The PSA signal gain (G) is defined as the ratio of the signal powers at the input ($z = 0$) and the output ($z = L$) of the waveguide as follows:

$$G \equiv \frac{\left[A_s(L)\right]^2}{\left[A_s(0)\right]^2}, \tag{18}$$

The calculated signal gain [Eq. (18)] is plotted in Fig. 2(a) as a function of the phase of the pump wave (ϕ_p). Note that a linear variation of the input pump phase corresponds to double the variation of the relative phase of $\theta(z)$ according to Eq. (16). The input powers of each interacting wave at the waveguide facet are assumed to be 33 dBm for the pump wave (P_p) and -4 dBm for the signal and idler wave (P_s, P_i), respectively. The results show that the maximum signal gain is 19.0dB and 30.1dB for the crystal lengths (L) of 30 mm and 50 mm, respectively. These correspond to peak-to-peak gain differences of 41.3dB and 48.4dB, respectively. As indicated in Fig. 2(a), the power flow from the pump to the signal and idler and vice versa depends on the relative phase, which means the possibility to realize a PSA whose gain depends on the phase of the input signal. Figure 2(b) shows the maximum and minimum PSA gain (maximum deamplification) and the PIA gain without the input idler power as a function of the input pump power for the 30-mm long device. As can be appreciated from the graph, the PSA gain increases quadratically as the pump power increases. The difference between PSA and PIA gain reaches the theoretical limit of ~ 6dB at the input pump power of 33 dBm, as indicated in Fig. 2(b) [30].

The maximum PSA signal gain is also plotted in Fig. 3(a) as a function of the crystal length for an input pump power of 33 dBm. The result clearly shows that the gain increases as the crystal length increases due to the longer interaction length. In particular, the maximum gain is proportional to the fourth-power of the crystal length until the PSA gain starts to saturate because of over-coupling between the pump wave and signal/idler waves. Figure 3(b) shows the calculated maximum PSA gain plotted as a function of the signal wavelength (λ_s - λ_p) at an input pump power of 33 dBm. The calculated 3-dB bandwidths are 88 nm and 77 nm for the crystal lengths of 30 mm and 50 mm, respectively. This indicates that the proposed PSA scheme is applicable to broadband operation and the amplification of multiple WDM data signals.

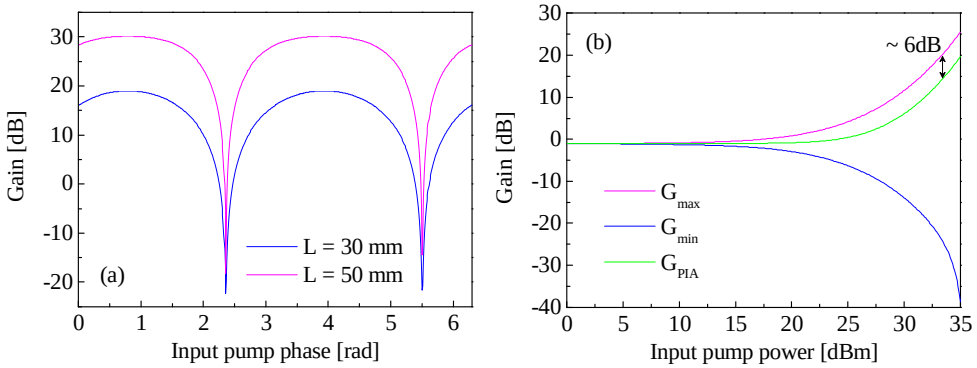

Fig. 2. (a) Calculated signal gain plotted as a function of the initial relative pump phase for a crystal length of 30 mm and 50 mm at an input pump power of 33 dBm, and (b) Variation of maximum, minimum PSA gain and PIA gain as a function of the input pump power for a crystal length of 30 mm.

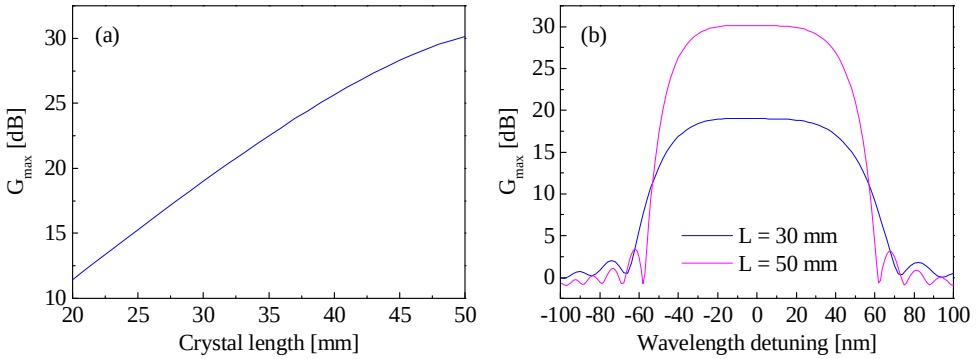

Fig. 3. (a) Maximum signal gain as a function of crystal length for an input pump power of 33 dBm, and (b) Calculated maximum PSA gain plotted as a function of the signal wavelength at an input pump power of 33 dBm.

3. Experimental results

Figure 4 shows the experimental setup that we used to validate the proposed PSA approach and associated model. It comprises two stages of PA. Firstly, a $\chi^{(3)}$-based fibre PA is used to generate a phase-locked but conjugated idler [15]. The resulting phase-locked pump, signal and idler waves were then passed through a device that allows a controlled adjustment of the relative phase between them, before being injected into a cascaded $\chi^{(2)}$-based PA (PPLN waveguide) used to obtain PSA operation. Two wavelength tunable continuous-wave (CW) lasers were used as the pump and the signal sources operating at 1546.0 nm and 1541.4 nm, respectively. The two beams were combined together into a single fibre at the input to the system using an arrayed waveguide grating (AWG). The pump-to-signal power ratio was set to ~ 20dB and the combined beams were launched into an amplitude modulator to generate

100-ps pulses at a repetition rate of 2.5 GHz, thereby allowing for a four-fold increase in the peak power of the signals after onward amplification in an EDFA. After amplification the signal and pump beams were coupled into a 500-m long highly nonlinear fibre (HNLF) with a nonlinear coefficient of $\gamma = 20$ $(W \cdot km)^{-1}$, a dispersion of 0.06 ps/nm/km, and a dispersion slope of 0.0035 ps/nm^2/km. The resulting three waves (pump, signal, and idler) were subsequently passed through an optical processor (Finisar Waveshaper 4000E) allowing for individual filtering, attenuation, and phase-shifting relative to each other. A polarizer, EDFA, and appropriate polarization control elements were used to amplify and align all three waves to the optical axis of the PPLN waveguide for the cSHG/DFG process. The total power at the waveguide input was 14 dBm (peak power of 20 dBm) with the pump signal completely dominating the power (coupling loss of ~ 1.4dB).

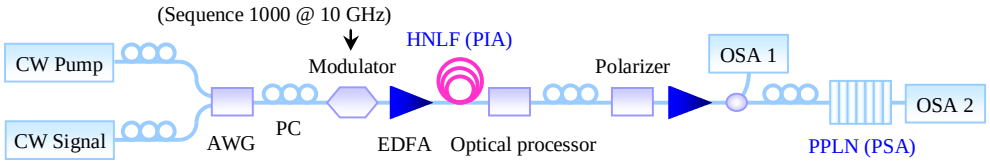

Fig. 4. Schematic for the proposed frequency non-degenerate PSA based on the cSHG/DFG process in the PPLN waveguide.

Figure 5(a) shows the measured output spectra for amplification and deamplification of the signal and idler wave. The maximum gain achievable for this pump power level was 0.65dB and the peak-to-peak signal gain variation was measured to be 3.4dB, which agrees well with the theoretical gain curve plotted in Fig. 5(b) as a function of the input pump phase. Note that the maximum gain/attenuation peaks occur at different absolute phases as compared to the ones shown in Fig. 2(a), since in the simulations we did not take account of the exact fibre length between the PSA and PIA. However, the gain profiles clearly indicate the phase-sensitive behaviour showing both the maximum amplification and deamplification with a period of π-phase. Note that the input and output coupling losses are not taken into account in measuring the gain. In the same figure we also report the corresponding PIA gain in the PPLN, i.e. in the absence of the input idler signal. To achieve this, the HNLF in the first stage was removed, while ensuring that the same absolute and relative power levels as in the PSA case were maintained at the input of the PPLN. As shown in Fig. 5(b), the difference between the PSA and PIA gain is about 1.7 dB. The negative PIA gain of ~ 1dB is due to the beam propagation loss (α) within the waveguide, which agrees well with the theoretical estimation at this input power level. The PIA gain also increases as expected as the input pump power increases, as shown in Fig. 2(b).

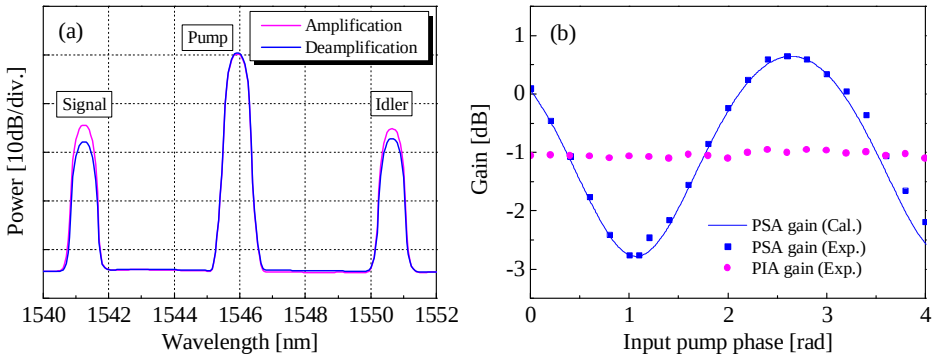

Fig. 5. (a) Measured output spectra of three interacting waves showing amplification and deamplification, and (b) the measured and calculated phase-sensitive gain plotted as a function of initial pump phase for PIA and PSA operation.

For these first proof-of-principle experiments, we kept the excitation levels of the PPLN waveguide well within the restrictions imposed by the pigtailing of this specific device (maximum input power of 14 dBm). Improvements in current pigtailing technology mean that currently available devices are now able to handle peak pulse powers of up to 33 dBm. In light of the excellent agreement between our first experiments and the theoretical predictions [Fig. 5(b)], we can reasonably expect to reach a differential PSA-PIA gain of ~ 6dB with a pump power of 33 dBm, as expected in Fig. 2(b), from state-of-the-art PPLN devices.

Finally we investigated broadband PSA operation. To do this, we tuned the CW signal source to the following central wavelengths: 1529.82 nm, 1534.47 nm, 1536.07 nm, and 1538.3 nm, respectively. Figure 6 shows the calculated and measured maximum and minimum PSA signal gain for each signal wavelength. As can be seen, the measured phase-sensitive gains were almost constant (with a variation of less than 0.5dB across the whole 16 nm wavelength range, which was limited by the tuning range of our input signal source). Since symmetric operation around the pump wavelength is expected, broadband operation of the process exceeding the 32 nm effective measurement bandwidth can be inferred. The theoretical device bandwidth predicted in Fig. 3(b) is 88 nm – significantly broader than can routinely be obtained for a fibre based single-pump, non-degenerate PSA.

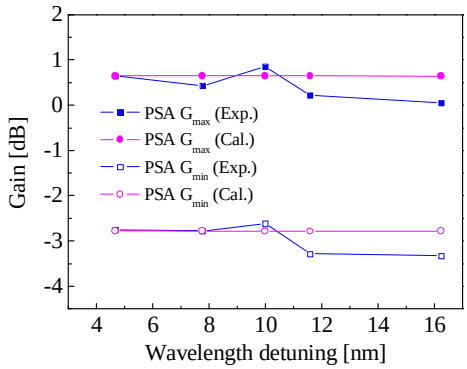

Fig. 6. Variation of the maximum and minimum points of the phase-sensitive signal gain for several signal wavelengths.

4. Conclusion

We have theoretically investigated and experimentally demonstrated, for the first time to our knowledge, a frequency non-degenerate PSA based on cSHG/DFG occurring in a single PPLN waveguide. The PSA performance was demonstrated and characterised by exploiting the combination of a $\chi^{(3)}$-based PIA to create the initial phase-locking among the waves followed by a $\chi^{(2)}$-based PSA based on the cSHG/DFG process. We verified the very good agreement between our theoretical predictions and the performance of the cSHG/DFG PSA, achieving a maximum gain of 0.65dB with a peak-to-peak gain variation of 3.4dB for a ~ 100-ps duration, 2.5 GHz pulsed signal in a 3-cm PPLN waveguide with an input pump of 14 dBm. Our first proof-of-principle experiments show also the potential of the process as a broadband PSA mechanism. Further significant improvements of the PSA gain can be envisaged with state-of-the-art PPLN technology, enabling higher pump powers. Our calculations show that PSA gains in excess of 30dB can be achieved in practical device lengths (50 mm) for launched power levels of 33 dBm. We highlight the compact size and the fact that no SBS suppression techniques are required as major advantages of the PPLN approach relative to silica fibre based PSA implementations.

Acknowledgement

The research leading to these results has received funding in part from the UK EPSRC under grant agreement EP/F032218/1 and the European Communities Seventh Framework Programme FP/2007-2013 under grant agreement 224547 (PHASORS).